Remote Sensing of Environment 233 (2019) 111417

Contents lists available at ScienceDirect

Remote Sensing of Environment

journal homepage: www.elsevier.com/locate/rse

A novel approach to monitoring wetland dynamics using CYGNSS: Everglades case study

Mary Morris[a,*], Clara Chew[b], John T. Reager[a], Rashmi Shah[a], Cinzia Zuffada[a]

[a] Jet Propulsion Laboratory, California Institute of Technology, Pasadena, CA, USA
[b] University Corporation for Atmospheric Research, Boulder, CO, USA

ARTICLE INFO

Keywords:
CYGNSS
Wetlands
GNSS-R
Everglades
Inundation

ABSTRACT

Global Navigation Satellite System-Reflectometry (GNSS-R) is a remote sensing technique that uses scattered navigation signals opportunistically for science applications. The Cyclone Global Navigation Satellite System (CYGNSS) is the first science-driven GNSS-R satellite mission. Although the CYGNSS mission is motivated and designed to better observe weather processes, the data are also useful for other applications, including surface hydrology. This paper aims to demonstrate that CYGNSS has a capability for frequent, high-resolution observations of the wetland dynamics across a wide range of timescales in the tropics. Using matched estimates of water depth from the Everglades Depth Estimation Network (EDEN), we develop methods for mapping inundation over the South Florida Everglades wetland region using CYGNSS data. CYGNSS enables inundation mapping at rapid timescales throughout the diverse Everglades ecosystem, and the data could be complementary to those of well-established observational platforms. The strengths of GNSS-R could be leveraged with the strengths of other techniques to enable studies of wetlands dynamically at short timescales.

1. Introduction

1.1. Motivation

Wetlands are characterized by inundated or saturated land, either permanently or intermittently, and support vegetation types that are adapted to saturated conditions. Water stored in wetlands is an important component of the terrestrial water cycle as it not only affects local hydrology and ecosystems, but also drives dynamic floodplain evolution and plays a significant role in the emission of global atmospheric methane (CH_4) (IPCC, 2013). Wetlands also act as natural flood mitigators, temporarily storing excess precipitation and runoff. Previous research and community working groups have highlighted the need for better observations and understanding of surface water distribution and ecosystems globally because the current observations are limited (e.g. Marburger and Bolten, 2004).

As the water cycle accelerates and intensifies in a changing climate (Syed et al., 2010; Durack et al., 2012), impacts on wetlands and thus CH_4 emissions are expected. Terrestrial surface water maps, particularly those with sufficient frequency to represent dynamic characteristics of inundated areas, are critical for studies of global hydrology, biology, and biogeochemical processes. Quantitative assessments that are complementary to modern day numerical land-surface and hydrology model development require characterization of wetland dynamics across a range of time and spatial scales: from days to years, and down to sub-km scales (Papa et al., 2010).

However, hydrologic processes are relatively less understood at the short temporal (hourly to daily) and small spatial (< 10 km) scales. For example, it is currently impossible—using existing methods or publicly available data products—to globally observe the evolution of soil moisture and surface water on scales < 25 km and shorter than 3 days, (e.g., McColl et al., 2017). Resolving surface hydrology on short time scales with fine spatial resolution is required for fully quantifying the global latent heat flux, for accurately capturing flood events, and for high-resolution land surface model development. Changes in wetland CH_4 emissions are determined by regional wetland hydrology that can be significantly impacted by changes in regional scale processes.

Moreover, the urgent need to monitor wetlands globally is emphasized by the rapid rate of wetland loss, and the Ramsar Convention (2015) calls for a wetlands inventory and impact assessment. Detailed knowledge of the extent and the change in the extent of wetlands is also important to the community of practice: stakeholders, city planners, decision makers, government agencies.

* Corresponding author at: Jet Propulsion Laboratory, 4800 Oak Grove Drive, M/S 168-314, Pasadena, CA 91109, USA.
E-mail address: mary.g.morris@jpl.nasa.gov (M. Morris).

https://doi.org/10.1016/j.rse.2019.111417
Received 31 January 2019; Received in revised form 30 August 2019; Accepted 9 September 2019

1.2. Existing techniques

Existing remote-sensing methods for wetland mapping include an array of different instruments systematically grouped into five categories: optical coarse resolution, optical fine resolution, optical/hyperspectral, passive microwave (radiometers) and active microwave (e.g. synthetic aperture radar, scatterometers). Since the late 1990s, numerous sensors have been launched and operated, from which datasets have been used to generate wetland maps and observe their changes. A number of global wetland products are available; Matthews and Fung (1987), Global Lakes and Wetlands Database (Lehner and Döll, 2004; Prigent et al., 2001), and SWAMPS (Schroeder et al., 2014). However, these products have limitations in high biomass wetlands and are more relevant for analysis on longer time scales (i.e. seasonal scales). All are insufficient to address the science targets identified here (Papa et al., 2010; IPCC, 2013). For example, terrestrial water surface monthly global maps are produced by aggregating multisensor data, yielding 0.25 deg. resolution products (GIEMS) from which downscaling is performed. GIEMS is applicable for analysis at the time and spatial scales representative of the observations.

In the near future, observation-based studies of Earth's hydrosphere will benefit from highly anticipated Earth science missions, but the observations from these planned platforms have some limitations. One example is the upcoming Surface Water and Ocean Topography (SWOT) mission. Carrying a Ka-band radar, SWOT will be able to map rivers and other terrestrial open water bodies at very high spatial resolution (< 100 m), but the repeat frequency of 22 days at low latitudes will not be sufficient for observing the rapid change in tropical surface water dynamics. Additionally, since SWOT can only sense inundated wetlands, SWOT will be unsuitable for monitoring wetlands that are characterized by saturated soil, rather than inundation. SWOT will only be able to detect a small fraction of total wetlands: inundated and open inland water bodies. Wetlands with geophysically complex characteristics are important to monitor, but current platforms are limited in their ability to sample rapidly, and sense non-inundated wetlands, through all vegetation types.

1.3. GNSS-R

Global Navigation Satellite Systems Reflectometry (GNSS-R) is a remote sensing technique that can be viewed as a multistatic radar where the transmitters are the existing navigation satellites, and the receiving systems are application dependent (Zavorotny et al., 2014). A typical receiving system, comprising a GNSS receiver and one or more down-looking antennas, collects GNSS transmitted, Earth-surface scattered signals in the (primarily) forward scattering direction from an area around the specular reflection points. A reflection measurement is created by cross correlating the transmitted signal along the propagation path with a reference signal (known as pseudorandom noise, or PRN, GNSS code). This bistatic radar concept takes advantage of the ever-increasing number of GNSS transmitting satellites, and given a constellation of receivers, yields many non-repeat track, pseudo-randomly distributed measurements with global coverage and rapid revisit time.

A key strength of the GNSS-R technique is that the reflected bistatic signal scatters primarily in the forward direction. Over inundated, non-vegetated land, forward-scattered signals are stronger than the back-scattered signal of monostatic radars researchers may be more familiar with (e.g. synthetic aperture radars or scatterometers).

In the last few years, GNSS-R data have been analyzed over a number of wetlands. The first set of GNSS-R observations from the TechDemoSat-1 (TDS-1) satellite (Jales and Unwin, 2015) showed potential for high sensitivity to surface water. Earlier studies have documented the ability of GNSS-R to reveal wetlands present in the Amazon basin; large increases in the peak value of received power indicate areas of vegetated wetlands or inland water bodies (Shah and Hajj, 2015; Zuffada et al., 2016; Chew et al., 2016; Jensen et al., 2018). An analysis of a variety of scenes—from the Ebro delta rice fields to the Mississippi wetlands—is presented and complemented by modeling in Nghiem et al. (2017). Remarkably, after TDS-1 data is corrected for known parameters, Nghiem et al. (2017) show that the difference in peak reflected power between inundated and dry flat terrains is ~ 10 dB—even when the wetlands are obstructed by thick vegetation. As TDS-1 is a technology demonstration, for a long time the reflectometry data were only available for 2 out of 8 days; the limited amount of data restricted thorough statistical studies, but provided a stepping-stone for future GNSS-R research.

1.4. Introduction to CYGNSS

The launch in December 2016 of Cyclone Global Navigation Satellite System (CYGNSS), a NASA Earth science Venture-class mission, has recently made available many more spaceborne data for understanding the GNSS-R technique (Ruf et al., 2016, 2018). CYGNSS consists of a constellation of eight small satellites distributed on a single orbit plane in low Earth orbit (LEO). The objective of the CYGNSS mission is to estimate near-surface wind speed in all precipitating conditions. In particular, CYGNSS is optimized to capture short-term weather processes, like the lifecycle of tropical cyclones. The mission's orbit inclination is 35°, resulting in a latitudinal coverage of about ± 39°, and enables the mission to target the region where most tropical cyclones develop. Due to the nature of the opportunistic signals, an exact revisit time is challenging to calculate (Bussy-Virat et al., 2019), but the CYGNSS constellation is designed to frequently sample a storm's wind field on hourly time scales.

Although the CYGNSS mission is motivated by the study of weather phenomena over the ocean, observations over land are also routinely collected and provided for scientific analysis. The L1A data product (Gleason et al., 2018) can be used over land to infer properties of the surface, including the presence of water. This paper aims to demonstrate that CYGNSS has a capability for frequent, high-resolution observations of the wetland dynamics across a wide range of timescales in the tropics. To demonstrate this capability we use ancillary data, described in Section 2, to explore the relationship between ground-based truth and CYGNSS data. As CYGNSS is just one GNSS-R mission, one that was not designed or intended for remote sensing of the land surface, the constellation cannot sample the surface fast enough to produce spatially complete, high-resolution maps of the land surface every day. However, the potential of GNSS-R data is illustrated in Section 3, alongside the methodology description, with examples of CYGNSS data aggregated over long timescales. Even so, results, described in Section 4, demonstrate that CYGNSS has the capability to capture changes in inundation, using sparsely-sampled data over shorter time periods. Considering all analysis documented here, Sections 5–6 summarize comparisons made between CYGNSS and ancillary datasets, and offer insights on the role GNSS-R could play in future missions.

2. Datasets

2.1. Ancillary data

Our study focuses on the Everglades—a natural region of tropical wetlands in the southern portion of the U.S.A. state of Florida (FL)—since there are a number of ancillary datasets available for comparison. The complex hydrology in the region is controlled by a number of factors: precipitation patterns, topography, surface geology, proximity to the coast, and the surrounding development of South Florida. Depending on the external and hydrologic forces at work, diverse sets of flora are sustained in the Everglades (Davis and Ogden, 1994). An example of the types of vegetation and land cover are illustrated in Fig. 1, using the basic classification system employed for the GAP/LANDFIRE National Terrestrial Ecosystems 2011 dataset (Homer

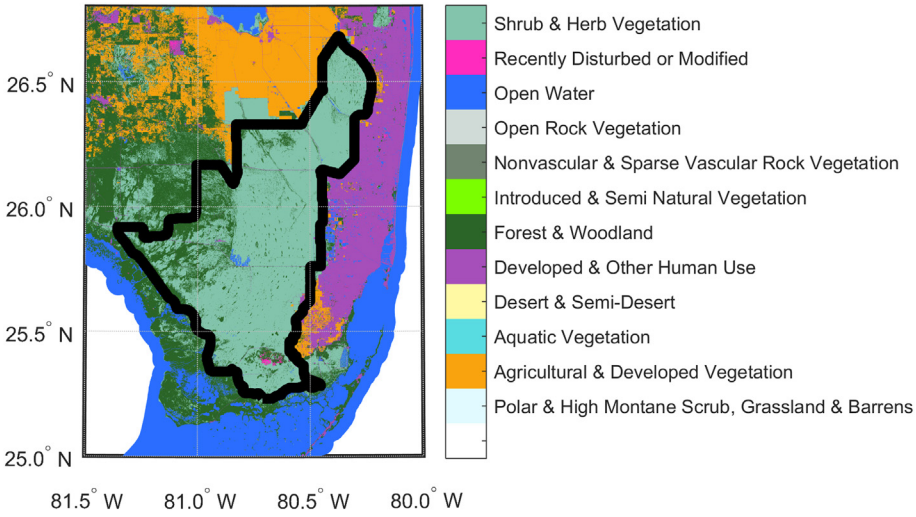

Fig. 1. Land classification in South Florida, as reported in the GAP/LANDFIRE National Terrestrial Ecosystems dataset published in 2011 (Homer et al., 2015). The black polygonal boundary denotes the Everglades Depth Estimation Network (EDEN) coverage area, the region of focus for this study.

et al., 2015). Flora of the Everglades consists primarily of shrub and herbaceous vegetation along with woodland and forest. Sitting on top of a porous bed of limestone, highly variable seasonal precipitation and the development of water control structures in conservation areas determine inundation extent. A detailed description of the developed structures that control the flow of water in the study area can be found in Telis et al. (2015). Where the landscape consists of ridges and sloughs, water will channel between ridges.

Although a complex landscape, the availability of ground truth makes analysis within the Everglades more tractable than in other wetland complexes. For example, the Everglades Depth Estimation Network (EDEN) provides a daily map of water depth estimates (Telis et al., 2015; Patino et al., 2018). Daily estimates of water depth are crucial for determining the usefulness of CYGNSS data for resolving inundation events at rapid timescales.

The spatial extent of EDEN is denoted by a black boundary polygon in Fig. 1 and an orange boundary polygon in Fig. 2, and includes all or parts of five water conservation areas, in addition to the Big Cypress National Preserve, the Pennsuco Wetlands, and the Everglades National Park. Water levels across the EDEN domain are computed by using the EDEN surface-water model (Patino et al., 2018). The surface-water model uses the daily median water level from 223 instrument stations with a digital elevation model of the land surface to estimate water depth. The EDEN water depth product provides estimates for each 400-m by 400-m grid cell across the domain.

Another dataset used for comparison here is the Pekel surface water product (Pekel et al., 2016). Derived from Landsat images (Wulder et al., 2016), Pekel et al. document changes in surface water since 1984, globally, with 30-m resolution. The Pekel products serve this study by providing a probabilistic map of surface water coverage for comparison with EDEN and CYGNSS-based analyses. An example of one Pekel product is shown in Fig. 2: a map of surface water occurrence (%). The surface water occurrence shown in Fig. 2 illuminates the hydrologic diversity within S. FL, with both permanent water bodies and dynamic wetland scenes within the Everglades complex.

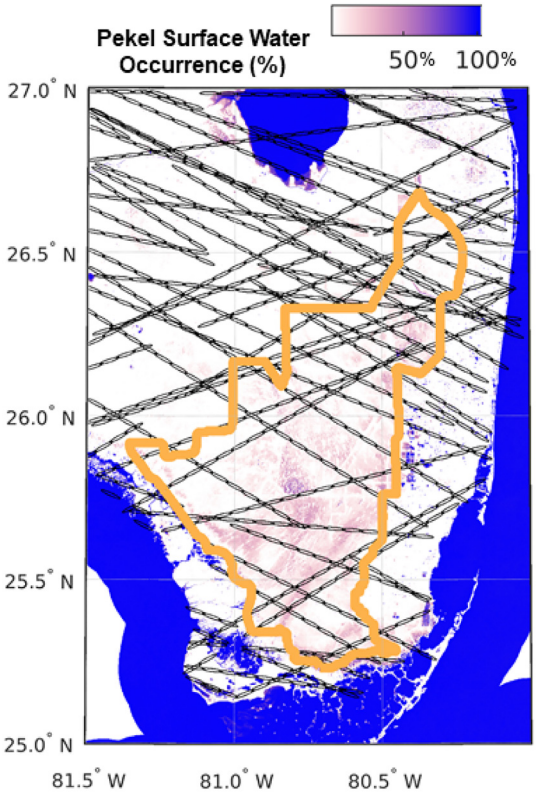

Fig. 2. A comparison of spatial coverage for the ancillary datasets used in this study, with a sample of CYGNSS coverage over 3 days. The map shows Pekel surface water dataset (blue hues), for S. Florida, USA, with tracks of CYGNSS data (collected from 04 to 06 June 2017) projected on top, and the area covered by the Everglades Depth Estimation Network (EDEN) outlined in orange. The CYGNSS footprint is approximated with a 1 × 7 km elliptical area on the surface, corresponding to incoherently summed measurements over 1 s. The background color map illustrates the percent water occurrence provided from the Pekel et al. (2016) surface water dataset. (For interpretation of the references to color in this figure legend, the reader is referred to the web version of this article.)

2.2. CYGNSS data

Unlike the spatially consistent nature of the two ancillary products described above, CYGNSS observes a region in series of pseudo-random tracks, as shown in Fig. 2. Fig. 2 displays CYGNSS coverage over a three-day timespan; each ellipse represents a single CYGNSS observation, approximated to have a 1 × 7 km elliptical footprint based upon the area of the first Fresnel zone (Nghiem et al., 2017) and 1-second averaging along-track. Signals reflected from wetlands are coherent, and thus the active scattering area is defined by the Fresnel zones and the spatial resolution is higher than the nominal 25-km ocean surface

wind speed product that the mission was designed to routinely provide. The calculated revisit time of an area from CYGNSS depends on a trade-off between spatial and temporal coverage (Bussy-Virat et al., 2019). For a complete image of the surface, CYGNSS data must be composited in time and space. While the measurement has a set resolution, for analysis, CYGNSS data are typically assigned to a specific spatial area or grid, to ensure a consistent spatial reference to compare to over time. Analysis over short time scales is possible, at the cost of one of two things: 1) a decrease in spatial resolution of the analysis reference grid, or 2) if the highest resolution reference grid is required for the application, a lack of complete spatial coverage. However, the CYGNSS constellation's high temporal sampling of a region, although incomplete spatially, can be leveraged for analysis of fast-paced events like flooding.

For this study, we use CYGNSS data from April 2017 through June 2018 to ensure adequate seasonal variety, and enough data for separate training and validation tasks. In addition to the corrections described later in Eq. (5), CYGNSS data are subject to additional quality control. Data using GPS block IIF are excluded from this study; there are large uncertainties in calibration of these data (Wang et al., 2019). Additionally, we exclude data flagged as having 'large spacecraft attitude' errors and/or black-body calibration data. (CYGNSS, 2018; Ruf et al., 2016)

3. Methodology

3.1. CYGNSS data processing

With the support from the two sets of ancillary data described in Section 2.1, this study explores the sensitivity of CYGNSS to surface water. We then create CYGNSS-based inundation maps of the Everglades.

Mapping surface water coverage with CYGNSS assumes that the reflected signal is primarily coherent, as observed in early analysis of waveform shape and high peak power values of delay-Doppler maps (DDM) for reflections over wetlands (Nghiem et al., 2017); this is a working assumption in the GNSS reflectometry community. Peak value of coherent scattered power is defined as:

$$P^{coh} = \frac{P^{tx}G^{tx}}{4\pi(R_{tx-sp} + R_{sp-rx})^2}\frac{G^{rx}\lambda^2}{4\pi}\Gamma \quad (1)$$

where P^{tx} is the transmitted power, G^{tx} is the gain of the transmitting antenna, G^{rx} is the gain of the receiving antenna, λ is the wavelength of the signal, R_{tx-sp} is the distance between the transmitter and the specular reflection point, R_{sp-rx} is the distance between the receiver and the specular reflection point, and Γ is the reflectivity of the surface. In order to solve for Γ, we assume that P^{tx} and G^{tx} are relatively constant over a short period, and remove the constant terms, obtaining:

$$P^{coh} \propto \frac{G^{rx}\Gamma}{(R_{tx-sp} + R_{sp-rx})^2} \quad (2)$$

Unfortunately, the peak power of the DDM is also affected by other variables like system noise levels and receiver instrument gain. We attempt to mitigate these factors by introducing an additional correction to calculate the signal-to-noise ratio (SNR). SNR is the peak power of the DDM normalized to a noise floor, which is defined as the mean cross-correlation value N before the leading edge of the reflection in the DDM:

$$SNR_{dB} = 10\log_{10}P^{coh} - 10\log_{10}N \quad (3)$$

and arrive at a function that describes the relationship between the signal to noise ratio (in dB) and the reflectivity:

$$SNR_{dB} \propto 10\log 10\Gamma, \quad (4)$$

As previously described by Chew et al. (2016, 2017a, 2017b), a corrected SNR (in dB) is constructed from the CYGNSS level-1 SNR data (SNR_{dB}) as:

$$SNRc = SNR_{dB} - G_{dB}^{rx} + 20\log 10(R_{tx-sp} + R_{sp-rx}) \quad (5)$$

where $G_{dB}{}^{rx}$ is the gain of the receiving antenna (in dB). After inspection of the data, we determined it is reasonable to assume incidence angle effects are negligible for this application. Our observable, SNRc, is directly related to the surface reflectivity but it absorbs all the approximations made above, and the fact that we do not know the proportionality factor in Eq. (4). For this analysis, the proportionality factor could include information related to surface properties that are unrelated to surface water: e.g. roughness, vegetation type, and vegetation water content. With increasing surface roughness and vegetation cover, we expect SNRc to decrease. With increasing vegetation water content, we expect SNRc to increase. The quantification of these sources of uncertainty remains the subject of future work. Fig. 3 shows the CYGNSS data plotted in Fig. 2, but now with color according to the processing described by Eq. (5). The magnitude of SNRc calculated from Eq. (5) is referenced to a value set by the CYGNSS project, but the absolute value is not important, only the relative changes matter. With an increase in SNRc (represented by bluer hues in Fig. 3), we expect wetter ground conditions. The highest values of SNRc plotted in Fig. 3 correspond to sites of highest surface water content. While the general location of the Everglades complex starts to take shape with just a few days of CYGNSS data, a composite of data over time gives a better sense of where wet and dry regions are generally located.

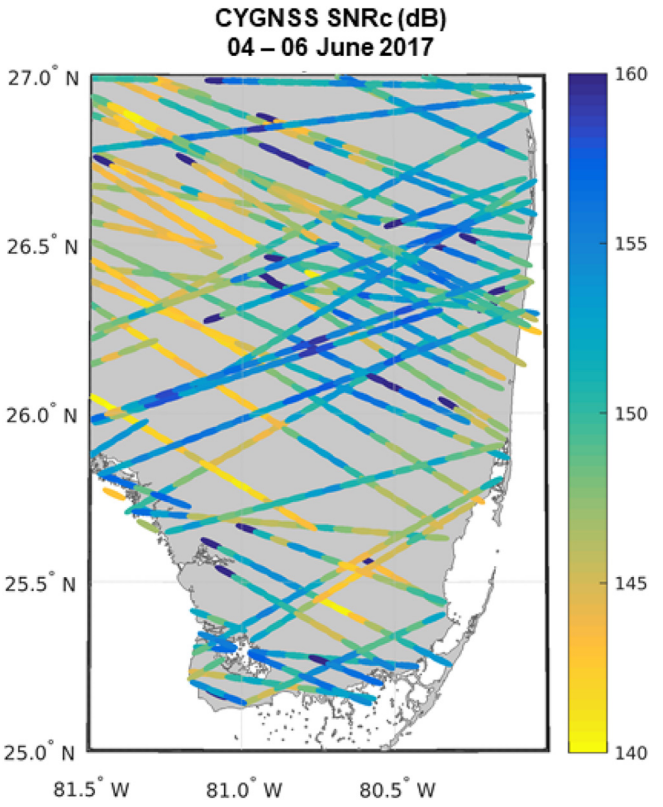

Fig. 3. Map of CYGNSS data (collected from 04 through 06 June 2017) projected as ellipses. The CYGNSS footprint is approximated with a 1 × 7 km elliptical area on the surface, corresponding to incoherently summed measurements over 1 s. Color represents the corrected SNR (SNRc; Eq. (5)) of the CYGNSS observation.

Fig. 4 visualizes a composite of CYGNSS data collected between April 2017 through March 2018. While the data were previously visualized as 1 × 7 km ellipses in Figs. 2–3, the data are assigned a grid box in Fig. 4 according to where the specular point falls. Areas with higher SNRc tend to have more instances of standing water over this

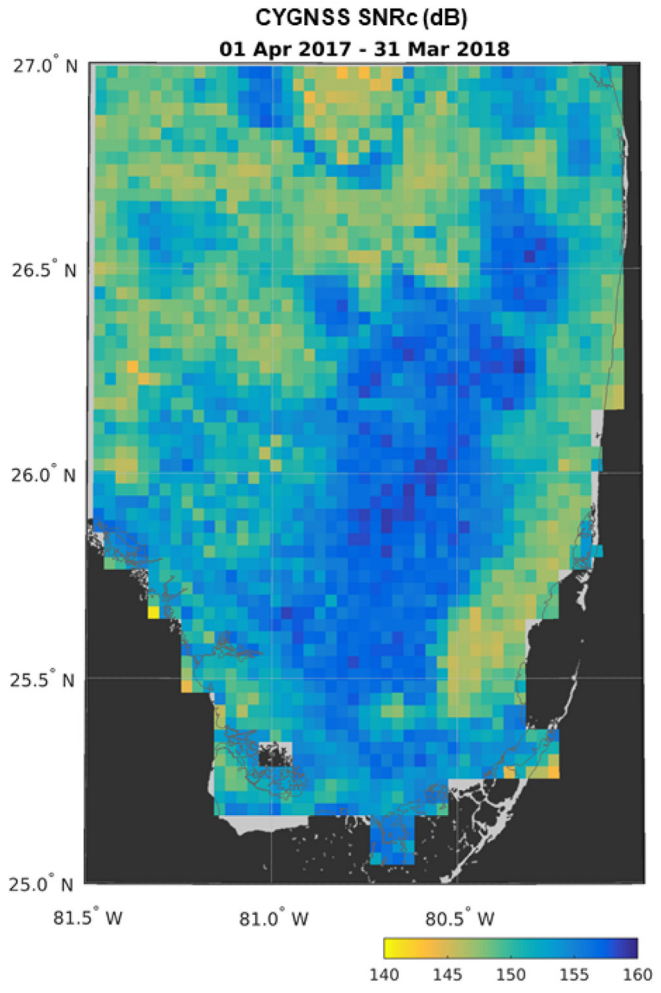

Fig. 4. Median SNRc (dB) (Eq. (5)) composited from April 2017 through March 2018, on a 0.03 × 0.03° grid over S. FL, USA.

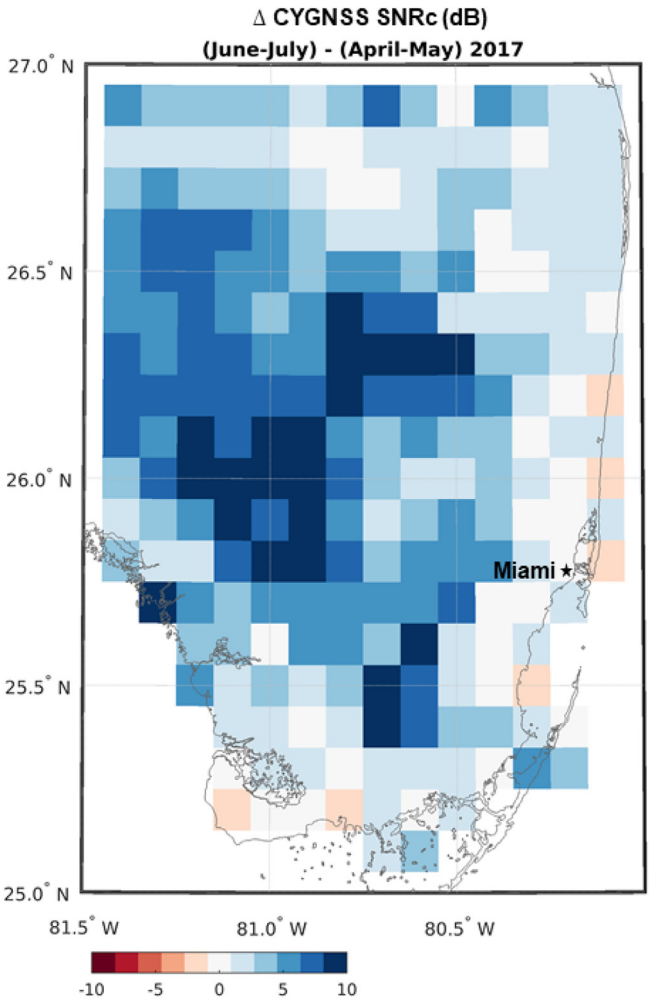

Fig. 5. Change in median CYGNSS SNRc from (April/May) to (June/July), over S. FL, USA, on a 0.1 × 0.1° grid.

time frame. However, there are seasonal changes in the Everglades water extent. For example, Fig. 5 highlights the difference in SNRc between a wet and dry period; we have gridded the data for this shorter time period at lower resolution, compared to Fig. 4, as there are fewer data available. The transition between the dry and wet seasons is responsible for the large increase in SNRc from April/May to June/July. The wet to dry season transition is evident in monthly precipitation data recorded for select Florida cities; Table 1 presents precipitation totals and departures from normal from April through July 2017. (Florida Climate Center, 2017)

Total rainfall increased in each city during each month from April through July, with notable positive departures recorded in Miami (location labeled in Fig. 5) in June and July. The Everglades region is dynamic, and the main objective of this study is to determine how to capture the dynamics of inundation with CYGNSS data collected over short time scales.

3.2. Threshold-based prediction of surface water

A number of studies have explored the relationship between CYGNSS SNRc to surface water (e.g. Zuffada et al., 2017; Chew et al., 2018; Lavalle et al., 2018). Initial attempts outlined in Zuffada et al. (2017) and Lavalle et al. (2018) explored the correlation between CYGNSS SNRc and the fraction of water in a CYGNSS footprint. More recently, Chew et al. (2018) developed a technique that relates a threshold change in SNRc to flood inundation extent. Here, similar to Chew et al. (2018), we relate CYGNSS SNRc to a binary prediction of surface water inundation.

Table 1
Precipitation totals and departures from normal (inches) for selected cities in Florida, from April through July 2017 (Florida Climate Center, 2017).

Station	Total rainfall (inches)				Departure from normal			
	April	May	June	July	April	May	June	July
Orlando	Trace	3.36	5.44	10.6	−2.68	−0.09	−2.14	3.33
Tampa	0.59	1.48	7.9	8.99	−1.44	−0.62	1.22	1.92
Miami	2.16	2.69	15.97	12.45	−0.98	−2.65	6.3	5.95

In order to determine a suitable threshold, CYGNSS SNRc is compared to water depth from EDEN from January 2018 through June 2018. For this analysis, we assumed water exists where the water depth is reported to be greater than zero, and does not exist otherwise. The EDEN water depth data are averaged to match the resolution of the assumed CYGNSS footprint. Comparing the SNRc data in categories of zero and above zero depth, we found that SNRc was generally lower for cases where depth was reportedly zero, as expected. Fig. 6 shows the cumulative distribution function (CDF) for data with water (depth above zero) and data without water (depth equal to zero). While there are overlaps between these two populations of data, half of the 'dry' SNRc data exists below 148 dB, while the large majority of 'wet' SNRc values are > 148 dB. Based on this comparison, our threshold is defined as 148 dB for this case study. If the reported CYGNSS SNRc value

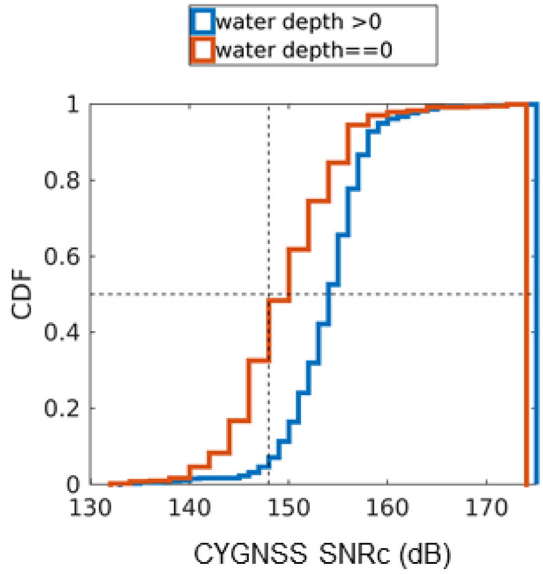

Fig. 6. CDFs of corrected CYGNSS SNRc over the Everglades Depth Estimation Network coverage area from January through June 2018. The blue line shows the data population collocated with EDEN depth estimates above zero (surface water assumed present). The red line shows the data population collocated with EDEN depth estimates equal to zero (surface water assumed absent). Crossed dashed lines show choice in CYGNSS threshold for determining a binary water/no-water choice. For this region, corrected CYGNSS SNRc < 148 dB is assumed to be dry. (For interpretation of the references to color in this figure legend, the reader is referred to the web version of this article.)

is < 148 dB, we assume no-water is in the CYGNSS footprint. If CYGNSS SNRc is above 148 dB, we assume some amount of surface water exists in the CYGNSS footprint. Since the populations overlap, the threshold method will perform poorly for instances where the reported SNRc is above 148, but the EDEN dataset says that the footprint is dry. This threshold methodology is a first step, to which additional complexity can be added in future work.

The overlap between CYGNSS and EDEN datasets limits the general applicability and robustness of the defined threshold method. Since EDEN covers a region that is often inundated, we have more data with an EDEN depth above zero, than not. Any thresholds defined here are specific to our case study, and enable an experiment from which future algorithm development can build on.

4. Results

To examine the usefulness of a threshold water mask, we look at data excluded from the dataset used for training and visualization in Fig. 6. First, we explore observations of an intense flooding event in S. Florida in early June 2017. Prior to this event, the region was characterized by dry conditions (see Table 1), and the Everglades water depths were low. A rain event, primarily spanning 05–07 June 2017, ended the dry season, and injected a large amount of water into the Everglades and surrounding area.

Figs. 7–8 compare data on the day before and after the heavy rain event. Fig. 7a shows the EDEN water depth map in color, with zero depth masked in grey, and a boundary placed around the main areas of above zero water depth. Fig. 7b shows CYGNSS SNRc tracks, for the same day, and with the corresponding above-zero-water-depth-boundary for reference across all subplots. Finally, Fig. 7c shows the Pekel water occurrence map for further context. Fig. 8 shows similar information, except for the day after the event. Prior to the event, water depth values (Fig. 7a) are lower, and the corresponding CYGNSS SNRc data alludes to drier conditions as well. After the event, water depth values (Fig. 8a) increase substantially, as do the CYGNSS SNRc observations.

We apply the threshold methods presented in Section 3.2 to obtain the CYGNSS-based water masks shown in Figs. 9b–10b. Figs. 9a–10a show the same EDEN water depth information as their parallels in Figs. 7a–8a. Figs. 9b–10b show the mapping from a CYGNSS SNRc to a prediction of surface water existence. While the water masks provided by the Pekel water occurrence dataset (Figs. 7c–8c) contain probabilistic information, we create a water mask interpolated to the EDEN grid, based upon occurrence > 1% for comparison, and this mask is visualized in Fig. 9c–10c. We interpolate the Landsat data to the EDEN grid by averaging the finer-scale Landsat water occurrence data at the spatial reporting interval of the EDEN grid. The Pekel-derived water mask does not contain temporal information available in the EDEN and CYGNSS datasets, but provides complete coverage of the entire area.

Figs. 9 and 10 show the usefulness of the simple CYGNSS-based water mask. In places where water depth is low, as they are before the flooding event, the CYGNSS data predicts 'no water'. After the rain event, inundation—as reported by EDEN—increases in depth and extent, as does the CYGNSS water mask.

While we do not have ground truth outside of the EDEN coverage area, using data collected from April 2017 through December 2017, we can characterize overall performance statistics of the CYGNSS-based inundation mapping presented here. For additional context, we compare performance of the Landsat-based water mask (Figs. 9c–10c) to the CYGNSS-based mask. Although each dataset has strengths and weaknesses, for this analysis we assume that EDEN is ground truth. Considering CYGNSS data over the EDEN coverage area, and the static Landsat water mask, we calculated the contingency statistics outlined in Table 2. Our objective is to predict inundation from both methods, and then compare these predictions to the matched EDEN water depth data, in order to determine regimes where one method outperforms another.

5. Discussion

The maps shown in Figs. 7–10 show an extreme case for which additional temporal sampling information from CYGNSS could add value in the analysis of surface water extent. However, CYGNSS data coverage is less complete and consistent spatially as compared with Pekel surface water maps. Looking at a larger set of data, we can identify strengths and weaknesses of each method (Table 2).

We use the following statistics to describe each method's performance. Probability of detection (POD) is defined as:

$$POD = \frac{hits}{hits + misses} \tag{5}$$

Probability of false detection (POFD) is defined as:

$$POFD = \frac{false\ alarms}{false\ alarms + correct\ negatives} \tag{6}$$

False alarm ratio (FAR) is defined as:

$$FAR = \frac{false\ alarms}{hits + false\ alarms} \tag{7}$$

Bias score is defined as:

$$Bias\ Score = \frac{hits + false\ alarms}{hits + misses} \tag{8}$$

Critical success index is defined as:

$$Critical\ Sucess\ Index = \frac{hits}{hits + misses + false\ alarms} \tag{9}$$

A more detailed discussion of these statistics is presented by Wilks (2011).

The differences in performance between both methods are found to be significant at the 99% level. A comparison of probability of detection (POD) in Table 2 shows that CYGNSS detected water better, compared

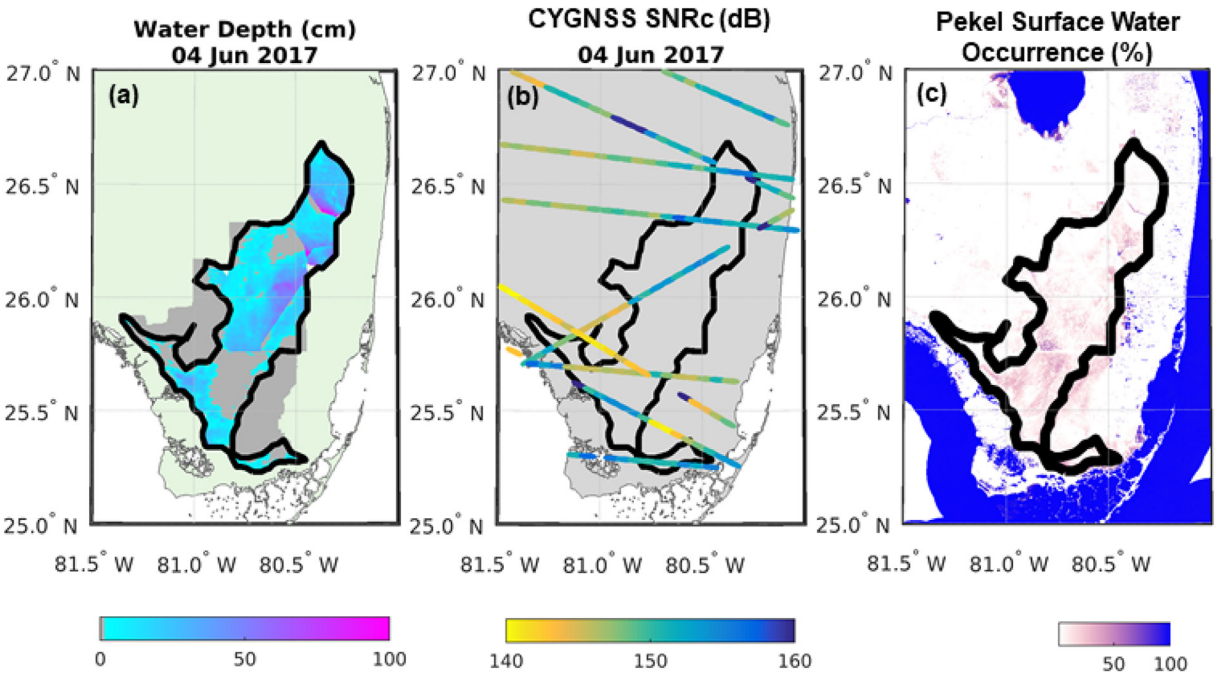

Fig. 7. An example of the scene before the record-setting rain event in S. FL—primarily taking place from 5 to 7 June 2017. (a) Water depth from EDEN on 04 June 2017, with a bold black boundary surrounding water depth data above zero. (b) CYGNSS SNRc (dB), with the same black boundary in (a) for comparison. (c) Pekel surface water occurrence, with the same black boundary for comparison.

with the simple > 1% water occurrence map we experimented with here. Both have a similar false alarm ratio. The Landsat-based method may have performed less well in terms of POD because it does not vary in time for this experiment. Landsat-based mapping of surface water could also be limited in scenes with dense vegetation, a known limitation of working at optical wavelengths. CYGNSS has strengths in penetrating vegetation because it uses the relatively longer 19 cm wavelength GPS signals. However, the limitations of GNSS-R in increasingly dense vegetated scenes remain the subject of future work. Additionally, CYGNSS has strengths in temporal sampling, which is useful for predicting inundation in cases that may not match up with the climatology represented in the Landsat-based map. The CYGNSS mission's constellation of spacecraft enables studies on shorter timescales, as compared with existing spaceborne platforms like Landsat.

In contrast, Landsat-based methods made proportionally more correct negative predictions. Therefore, as compared with CYGNSS, Landsat has a lower probability of false detection (POFD). CYGNSS performs less well at correctly predicting dry cases—likely a

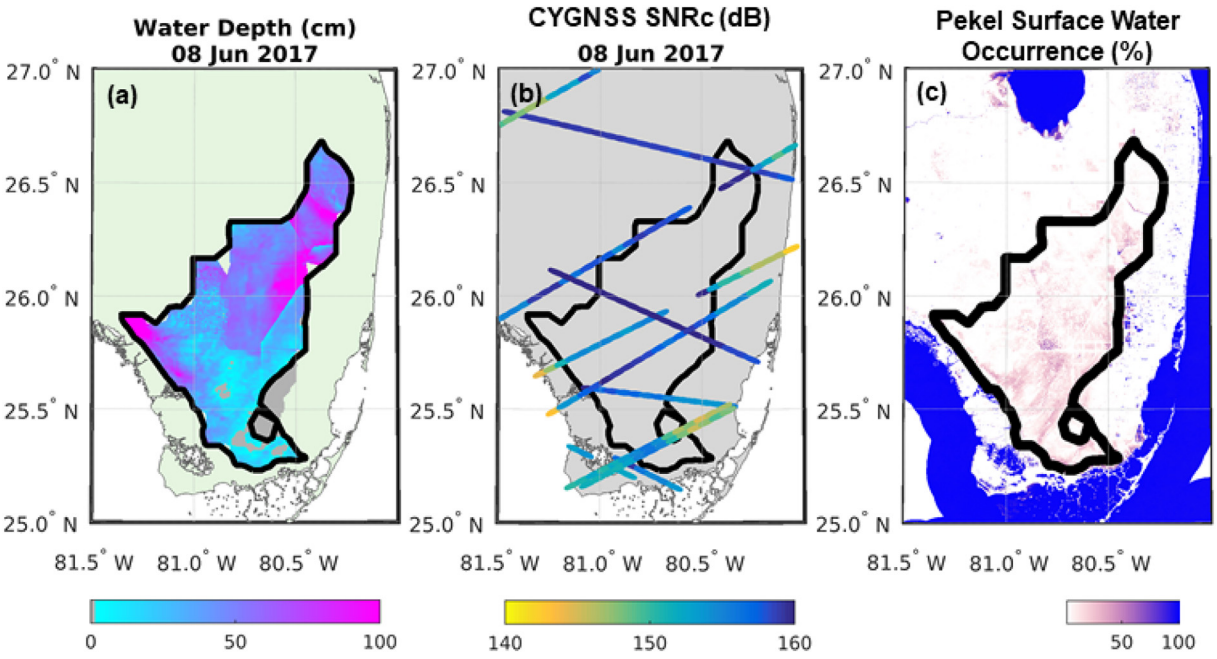

Fig. 8. An example of the scene after the record-setting rain event in S. FL—primarily taking place from 5 to 7 June 2017. (a) Water depth from EDEN on 08 June 2017, with a bold black boundary surrounding water depth data above zero. (b) CYGNSS SNRc (dB), with the same black boundary in (a) for comparison. (c) Pekel surface water occurrence, with the same black boundary for comparison.

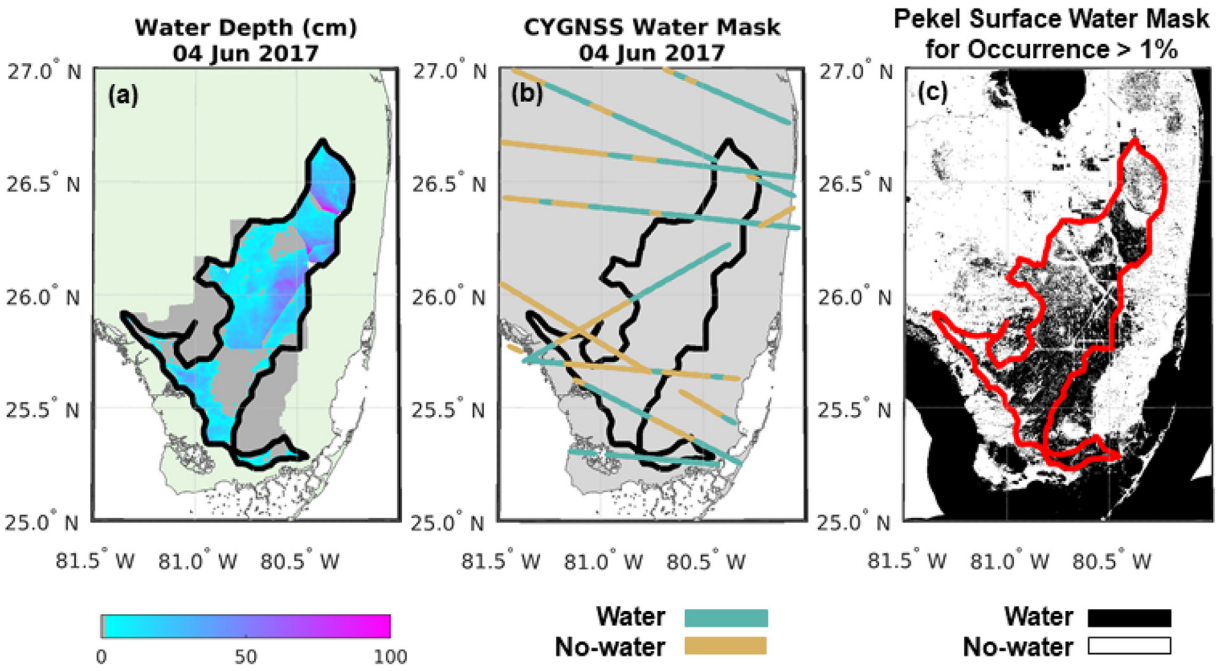

Fig. 9. An example of the scene before the record-setting rain event in S. FL—primarily taking place from 5 to 7 June 2017. (a) Water depth from EDEN on 04 June 2017, with a bold black boundary surrounding water depth data above zero. (b) CYGNSS-derived water mask, with the same black boundary in (a) for comparison. (c) Pekel surface water occurrence mask, assuming water exists where occurrence > 1%, with the same black boundary for comparison.

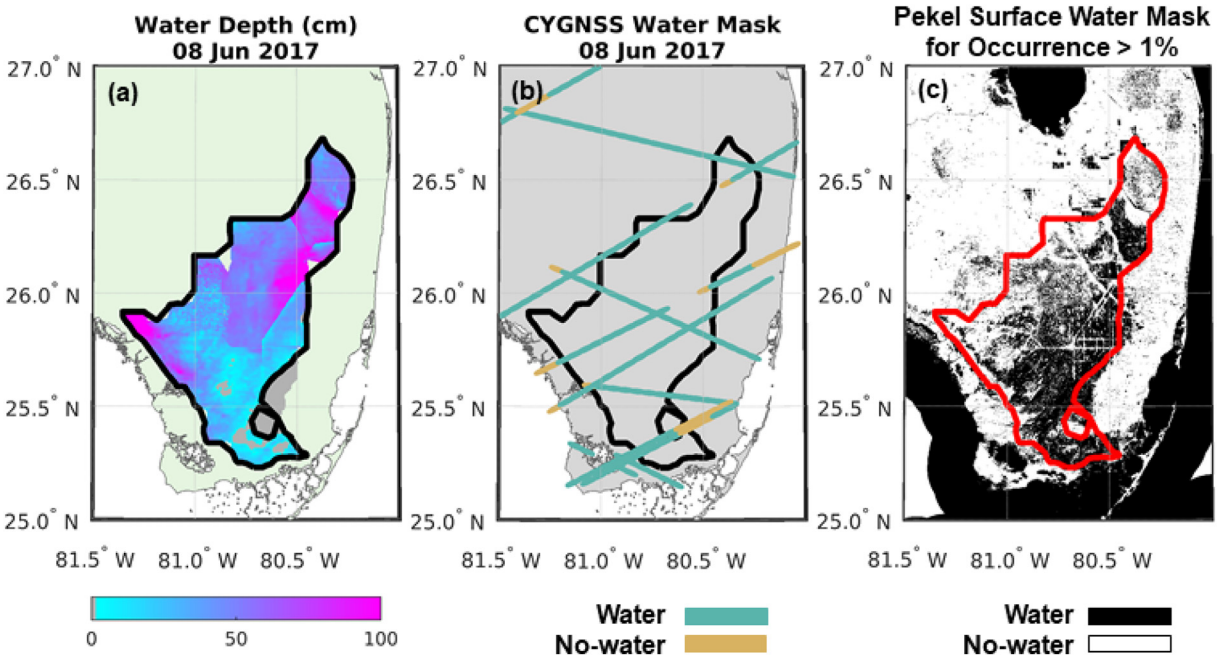

Fig. 10. An example of the scene after the record-setting rain event in S. FL—primarily taking place from 5 to 7 June 2017. (a) Water depth from EDEN on 08 June 2017, with a bold black boundary surrounding water depth data above zero. (b) CYGNSS-derived water mask, with the same black boundary in (a) for comparison. (c) Pekel surface water occurrence mask, assuming water exists where occurrence > 1%, with the same black boundary for comparison.

Table 2
Number of hits, misses, correct negatives, false alarms, probability of detection (POD), probability of false detection (POFD), false alarm ratio (FAR), bias score, and critical success index calculated for CYGNSS- and Landsat-based inundation prediction methods against EDEN from April through December 2017.

	Hits ($\#\times10^6$)	Misses ($\#\times10^6$)	Correct negatives ($\#\times10^6$)	False alarms ($\#\times10^6$)	POD	POFD	FAR	Bias score	Critical success index
CYGNSS	2.2	0.2	0.8	0.4	0.91	0.83	0.15	1.06	0.78
Landsat	5.8	5.0	1.1	1.0	0.54	0.48	0.14	0.63	0.49

consequence of a number of potential factors. For starters, our methods may not be robust enough to perform well in all situations. Assumptions made about the spatial extent for which CYGNSS is sensitive to surface water may need further examination (Loria et al., 2018); water outside the assumed CYGNSS footprint may be contaminating these results. The methods developed here could also be unable to differentiate between scenes containing saturated soil vs. inundation. With more analysis and increased understanding of the CYGNSS data over land, we anticipate improved performance in this category.

We emphasize that the purpose of this study is not to declare one method superior, but to examine differences in performance. For example, the bias score represents a ratio of (hits + false alarms) to (hits + misses). CYGNSS is more susceptible to false alarms, and Landsat is more susceptible to misses. Another metric considered here is the critical success index, calculated as the ratio of hits to (hits + misses + false alarms). Relative to the sum of hits, misses, and false alarms, CYGNSS has relatively more hits for this experiment. Strengths and weaknesses between techniques counter each other, and combining information from CYGNSS and Landsat could be complementary.

6. Conclusions

This paper describes a preliminary CYGNSS-based method for mapping inundation, which is tested on a relatively well-understood and instrumented wetlands complex—the Everglades. We found that CYGNSS data are useful for predicting inundation. Additionally, we showed that CYGNSS, comprised of a constellation of spacecraft, is able to capture dynamics of wetlands on rapid timescales. Although CYGNSS is compared here to a Landsat-based surface water map (Pekel et al., 2016), our intent is not to claim CYGNSS is more useful than Landsat for this application. Rather, we note that the increased temporal sampling from CYGNSS could complement well-established techniques that are unable to capture dynamic wetland scenes. The GNSS-based techniques are also less sensitive to vegetation and more sensitive to saturated soils, and therefore are useful where other techniques are more limited. The data from CYGNSS are complementary to existing observational platforms, and future work will explore methods for synergizing different data to balance strengths and weaknesses.

Acknowledgements

The authors gratefully acknowledge support from the CYGNSS Science Team. This work was supported as part of the CYGNSS Competed Science Team and funded in part by NASA award no. 80NSSC18K1430, and NASA award NNH17ZDA001N-THP. A part of the work described in this paper was carried out by the Jet Propulsion Laboratory, California Institute of Technology under a contract with the National Aeronautics and Space Administration. Government sponsorship acknowledged.

References

Bussy-Virat, C.D., Ruf, C.S., Ridley, A.J., Jan 2019. Relationship between temporal and spatial resolution for a constellation of GNSS-R satellites. IEEE J. Sel. Topics Appl. Earth Obs. Remote Sens. 12 (1), 16–25 (doi: 0.1109/JSTARS.2018.2833426).

Chew, C., Shah, R., Zuffada, C., Hajj, G., Masters, D., Mannucci, A.J., 2016. Demonstrating soil moisture remote sensing with observations from the UK TechDemoSat-1 satellite mission. Geophys. Res. Lett. 43 (7), 3317–3324.

Chew, C., Colliander, A., Shah, R., Zuffada, C., Burgin, M., 2017a. The sensitivity of ground-reflected GNSS signals to near-surface soil moisture, as recorded by space-borne receivers. In: 2017 IEEE International Geoscience and Remote Sensing Symposium (IGARSS). IEEE, pp. 2661–2663 (July).

Chew, C., Lowe, S., Parazoo, N., Esterhuizen, S., Oveisgharan, S., Podest, E., Zuffada, C., Freedman, A., 2017b. SMAP radar receiver measures land surface freeze/thaw state through capture of forward-scattered L-band signals. Remote Sens. Environ. 198, 333–344.

Chew, C., Reager, J.T., Small, E., 2018. CYGNSS data map flood inundation during the 2017 Atlantic hurricane season. In: Scientific Reports. vol. 8. Nature Publisher Group, pp. 1–8.

CYGNSS, 2018. CYGNSS Level 1 Science Data Record Version 2.1. Ver. 2.1. PO.DAAC, CA, USA. Dataset accessed at. https://doi.org/10.5067/CYGNS-L1X21.

Davis, S.M., Ogden, J.C., 1994. Everglades: The Ecosystem and its Restoration. St. Lucie Press, Boca Raton, Florida, USA.

Durack, P.J., Wijffels, S.E., Matear, R.J., 2012. Ocean salinities reveal strong global water cycle intensification during 1950 to 2000. science 336 (6080), 455–458.

Florida Climate Center, 2017. Monthly Climate Summaries for Florida. https://climatecenter.fsu.edu/products-services/summaries, Accessed date: 28 January 2019.

Gleason, S., Ruf, C., O'Brien, A., McKague, D.S., 2018. The CYGNSS level 1 calibration algorithm and error analysis based on on-orbit measurements. IEEE J. Sel. Topics Appl. Earth Obs. Remote Sens. https://doi.org/10.1109/JSTARS.2018.2832981.

Homer, C.G., Dewitz, J.A., Yang, L., Jin, S., Danielson, P., Xian, G., Coulston, J., Herold, N.D., Wickham, J.D., Megown, K., 2015. Completion of the 2011 National Land Cover Database for the conterminous United States-representing a decade of land cover change information. Photogramm. Eng. Remote. Sens. 81 (5), 345–354. http://www.asprs.org/a/publications/pers/2015journals/PERS_May_2015/HTML/index.html#346/.

IPCC, 2013. Climate change 2013: the physical science basis. In: Stocker, T.F., Qin, D., Plattner, G.K., Tignor, M., Allen, S.K., Boschung, J., Nauels, A., Xia, Y., Bex, V., Midgley, P.M. (Eds.), Intergovernmental Panel on Climate Change, Working Group I Contribution to the IPCC Fifth Assessment Report (AR5), 2013. vol. 25 Cambridge Univ Press, New York.

Jales, P., Unwin, M., 2015. Mission description-GNSS reflectometry on TDS-1 with the SGR-ReSI. In: Tech. Rep. SSTL Rep, 248367. Surrey Satellite Technol. Ltd., Guildford, UK.

Jensen, K., McDonald, K., Podest, E., Rodriguez-Alvarez, N., Horna, V., Steiner, N., 2018. Assessing L-band GNSS-reflectometry and imaging radar for detecting sub-canopy inundation dynamics in a tropical wetlands complex. Remote Sens. 2018. https://doi.org/10.3390/rs10091431.

Lavalle, M., Morris, M., Shah, R., Zuffada, C., Nghiem, S.V., Chew, C., Zavorotny, V.U., 2018, July. Bistatic scattering modeling for dynamic mapping of tropical wetlands with CYGNSS. In: IGARSS 2018–2018 IEEE International Geoscience and Remote Sensing Symposium. IEEE, pp. 239–242.

Lehner, B., Döll, P., 2004. Development and validation of a global database of lakes, reservoirs and wetlands. J. Hydrol. 296 (1–4), 1–22.

Loria, E., O'Brien, A., Gupta, I., 2018. Detection & Separation of coherent reflections in GNSS-R measurements using CYGNSS data. 2018 IEEE International Geoscience and Remote Sensing Symposium (IGARSS), Valencia 3995–3998.

Marburger, J.H., Bolten, J.B., 2004. Administration research and development budget priorities. In: Memo. M-04. vol. 23.

Matthews, E., Fung, I., 1987. Methane emission from natural wetlands: global distribution, area, and environmental characteristics of sources. Glob. Biogeochem. Cycles 1 (1), 61–86.

McColl, K.A., Alemohammad, S.H., Akbar, R., Konings, A.G., Yueh, S., Entekhabi, D., 2017. The global distribution and dynamics of surface soil moisture. Nat. Geosci. 10 (2), 100.

Nghiem, S.V., Zuffada, C., Shah, R., Chew, C., Lowe, S.T., Mannucci, A.J., Cardellach, E., Brakenridge, G.R., Geller, G., Rosenqvist, A., 2017. Wetland monitoring with Global Navigation Satellite System reflectometry. Earth and Space Science 4 (1), 16–39 (Jan 1).

Papa, F., Prigent, C., Aires, F., Jimenez, C., Rossow, W.B., Matthews, E., 2010. Interannual variability of surface water extent at the global scale, 1993–2004. Journal of Geophysical Research: Atmospheres 115 (D12).

Patino, Eduardo, Conrads, Paul, Swain, Eric, Beerens, James, 2018. Everglades depth estimation network (EDEN)—a decade of serving hydrologic information to scientists and resource managers (ver. 1.1, January 2018). In: U.S. Geological Survey Fact Sheet 2017–3069, https://doi.org/10.3133/fs20173069. 6 p.

Pekel, J.F., Cottam, A., Gorelick, N., Belward, A.S., 2016. High-resolution mapping of global surface water and its long-term changes. Nature 540 (7633), 418.

Prigent, C., Matthews, E., Aires, F., Rossow, W.B., 2001. Remote sensing of global wetland dynamics with multiple satellite data sets. Geophys. Res. Lett. 28 (24), 4631–4634.

Ramsar Convention, 2015. Resolution XII.5 (Annex 3), 1–9 June 2015, Punta del Este, Uruguay. http://www.ramsar.org/sites/default/files/documents/library/cop12_res05_new_strp_e_0.pdf, Accessed date: 1 January 2019.

Ruf, C., Chang, P., Clarizia, M.P., Gleason, S., Jelenak, Z., Murray, J., Morris, M., Musko, S., Posselt, D., Provost, D., Starkenburg, D., 2016. CYGNSS Handbook. Ann Arbor, MI, Michigan Pub., ISBN, pp. 971–978.

Ruf, C.S., Chew, C., Lang, T., Morris, M.G., Nave, K., Ridley, A., Balasubramaniam, R., 2018. A new paradigm in earth environmental monitoring with the CYGNSS small satellite constellation. Sci. Rep. https://doi.org/10.1038/s41598-018-27127-4.

Schroeder, R., McDonald, K.C., Chapman, B., Jensen, K., Podest, E., Tessler, Z., Bohn, T.J., Zimmerman, R., 2014. Development and evaluation of a multi-year inundated land surface data set derived from active/passive microwave remote sensing data. Remote Sens. 7, 16668–16732.

Shah, R., Hajj, G.A., 2015. Assessment of GPS reflectometry from TechDemoSat-1 for scatterometry and altimetry applications. In: AGU Fall Meeting Abstracts, December.

Syed, T.H., Famiglietti, J.S., Chambers, D.P., Willis, J.K., Hilburn, K., 2010. Satellite-based global ocean mass balance reveals water cycle acceleration and increasing continental freshwater discharge, 1994–2006. Proc. Natl. Acad. Sci. U. S. A. 107 (42), 17916.

Telis, P.A., Xie, Z., Liu, Z., Li, Y., Conrads, P., 2015. The Everglades Depth Estimation Network (EDEN) Surface-Water Model, Version 2 (No. 2014–5209). US Geological Survey.

Wang, T., Ruf, C.S., Block, B., McKague, D.S., Gleason, S., 2019. Design and performance of a GPS constellation power monitor system for improved CYGNSS L1B calibration. In: IEEE Journal of Selected Topics in Applied Earth Observations and Remote

Sensing. vol. 12, no. 1. pp. 26–36.
Wilks, D.S., 2011. Statistical Methods in the Atmospheric Sciences, 3rd. edition. Academic Press (676 pp).
Wulder, M.A., et al., 2016. The global Landsat archive: status, consolidation, and direction. Remote Sens. Environ. (0034-4257) 185, 271–283. https://doi.org/10.1016/j.rse.2015.11.032.
Zavorotny, V.U., Gleason, S., Cardellach, E., Camps, A., 2014. Tutorial on remote sensing using GNSS bistatic radar of opportunity. IEEE Geosci. Remote Sens. 2, 8–45. https://doi.org/10.1109/MGRS.2014.2374220.
Zuffada, C., Chew, C., Nghiem, S.V., Shah, R., Podest, E., Bloom, A.A., Koning, A., Small, E., Schimel, D., Reager, J.T., Mannucci, A., 2016, August. Advancing wetlands mapping and monitoring with GNSS reflectometry. In: Living Planet Symposium. vol. 740. pp. 83.
Zuffada, C., Chew, C., Nghiem, S.V., 2017. GNSS-R algorithms for wetlands observations. In: IGARSS 2017–2017 IEEE International Geoscience and Remote Sensing Symposium, pp. 1126–1129 (Fort Worth, TX).